Steel and Composite Structures, *Vol. 20, No. 5 (2016) 1155-1171*
DOI: http://dx.doi.org/10.12989/scs.2016.20.5.1155

Demands and distribution of hysteretic energy in moment resistant self-centering steel frames

Arturo López-Barraza [*1], Sonia E. Ruiz [2a],
Alfredo Reyes-Salazar [1b] and Edén Bojórquez [1c]

[1] *Facultad de Ingeniería, Universidad Autónoma de Sinaloa, Culiacán, Sinaloa, México*
[2] *Instituto de Ingeniería, Universidad Nacional Autónoma de México, México City, México*

(*Received December 01, 2012, Revised July 08, 2015, Accepted October 19, 2015*)

Abstract. Post-tensioned (PT) steel moment resisting frames (MRFs) with semi-rigid connections (SRC) can be used to control the hysteretic energy demands and to reduce the maximum inter-story drift (γ). In this study the seismic behavior of steel MRFs with PT connections is estimated by incremental nonlinear dynamic analysis in terms of dissipated hysteretic energy (E_H) demands. For this aim, five PT steel MRFs are subjected to 30 long duration earthquake ground motions recorded on soft soil sites. To assess the energy dissipated in the frames with PT connections, a new expression is proposed for the hysteretic behavior of semi-rigid connections validated by experimental tests. The performance was estimated not only for the global E_H demands in the steel frames; but also for, the distribution and demands of hysteretic energy in beams, columns and connections considering several levels of deformation. The results show that E_H varies with γ, and that most of E_H is dissipated by the connections. It is observed in all the cases a log-normal distribution of E_H through the building height. The largest demand of E_H occurs between 0.25 and 0.5 of the height. Finally, an equation is proposed to calculate the distribution of E_H in terms of the normalized height of the stories (h/H) and the inter-story drift.

Keywords: steel frames; self-centering; semi-rigid connections; hysteretic energy; inter-story drift; time history analysis

1. Introduction

Post-tensioned steel moment resisting frames are structural systems proposed in recent years as an appropriate alternative to welded connections of moment resisting frames (MRFs) in seismic zones (Ricles *et al*. 2001, 2002, 2010, Christopoulos and Filiatrault 2002, Christopoulos *et al*. 2002, 2003, Garlock *et al*. 2005, 2007, 2008, Kim and Christopoulos 2009, Chung *et al*. 2009, Wolski *et al*. 2009, Tong *et al*. 2011, Zhou *et al*. 2014). They are designed to prevent brittle fractures in the area of the nodes of steel frames, which can cause severe reduction in their ductility capacity, as occurred in many cases during the 1994 Northridge and the 1995 Kobe

∗Corresponding author, Professor, E-mail: alopezb@uas.edu.mx
[a] Professor, E-mail: sruizg@iingen.unam.mx
[b] Professor, E-mail: reyes@uas.edu.mx
[c] Professor, E-mail: eden@uas.edu.mx

http://www.techno-press.org/?journal=scs&subpage=6 ISSN: 1229-9367 (Print), 1598-6233 (Online)

earthquakes. Under the action of an intense earthquake motion, beams and columns remain essentially elastic concentrating the damage on the energy dissipating elements, which can be easily replaced at low cost. Moreover, they provide capacity of energy dissipation and self-centering reducing the residual displacements. It is important to consider the residual displacements on buildings after a seismic event, as they may require heavy spending on repairs or the total demolition in the case of excessive structural damage. Recent studies of steel frames have shown that the maximum and residual drifts of PT steel MRFs are up to 50% of those of equivalent frames with welded connections (Hu and Zhang 2013, López-Barraza *et al*. 2013).

Although the maximum inter-story drift is one of the main parameters used in seismic design codes to guarantee a satisfactory seismic performance of structures, this parameter does not explicitly consider the effect of cumulative structural damage due to plastic deformation. It is pointed out that such structural damage can be properly accounted by using the concept of dissipated hysteretic energy (E_H). The estimation of hysteretic energy demands is especially important for structures subjected to long duration earthquake ground motions such as those occurring in the Valley of Mexico (Terán-Gilmore 2001, Bojórquez and Ruiz 2004). Some researchers have proposed seismic design methodologies that consider the cumulative effect of plastic deformation demands and the effect of the duration on the structural response (Akiyama 1985, Cosenza and Manfredi 1996, Terán-Gilmore 1996, Hancock and Bommer 2006). One way to explicitly consider the accumulated damage is through concepts of seismic energy. Methods based on energy concepts are oriented to provide a system with energy capacity greater than or equal to the energy demanded by the earthquakes (Uang and Bertero 1990). Seismic design methodologies exclusively based on dissipated hysteretic energy have been developed (Akbas *et al*. 2001, Choi and Shen 2001, Choi and Kim 2006, Bojórquez *et al*. 2008, Choi and Kim 2009) and damage indicators based only on E_H have been proposed (Terán-Gilmore and Jirsa 2005, Bojórquez *et al*. 2010), since E_H is closely related to structural damage. A very important aspect of the hysteretic energy, when it is used as a structural performance parameter is its distribution through the height of the building. Several researchers have proposed some alternatives regarding the way of E_H is distributed in steel structures but they are exclusively applied to MRFs. For example, Akbas *et al*. (2001) proposed to use a linear distribution of hysteretic energy along the height. Studies conducted by Bojórquez and Rivera (2008) in steel frames with rigid connections, suggested that when the energy dissipated by plastic behavior is concentrated in the beams of a structural framework, a log-normal function represents the form in which the energy is dissipated through the height.

In this paper the E_H of PT steel MRFs is estimated, several steel building models are considered. The frames are designed so that the demands of E_H focus on the dissipater elements placed (angles) in the connections, while beams and columns remain essentially elastic. However, the demands of E_H in columns and beams are also estimated. In order to calculate E_H in the post-tensioned semi-rigid connections, new equations that accurately represent the hysteretic cycles are proposed. These equations were validated by experimental tests carried out by the authors and other researchers (Garlock *et al*. 2005). The proposed expressions represent continuous functions that depend only on a few parameters in order to facilitate their use. Additionally, equations are proposed to calculate the distribution factors for hysteretic energy through height (F_{EH}), which depend on the maximum inter-story drift demands. Finally, it is important to say that the estimation of the hysteretic energy distribution through the height is a key issue to propose seismic design procedures of buildings based on hysteretic energy spectra (Bojórquez *et al*. 2008).

2. Structural models

2.1 Self-centering steel frames

The hysteretic energy distribution along the height is characterized by a factor which is obtained from the analysis of five post-tensioned steel frames. The semi-rigid connection is achieved by connecting the flanges in tension and compression of the beams to the column flanges by using bolted angles (TS, top and seat connection); these angles dissipate energy through hysteretic behavior in the connection. To design the five steel MRFs with PT connections, a procedure proposed by Garlock *et al*. (2007) is used where beams and columns of the frame are designed by considering the connections as rigid. Then, connections and post-tensioning elements are designed to meet service and resistance requirements. The frames were designed according to the seismic regulations of the Mexican City Building Code (MCBC 2004). The structures, which are used as office occupancy buildings, are supposed to be located on soft soils of Mexico City. They are 4-, 6-, 8-, 10- and 14- story buildings having 3 bays, hereafter identified as F4PT, F6PT, F8PT, F10PT and F14PT, respectively. Their fundamental periods (T_1) are 0.89, 1.03, 1.25, 1.37 and 2.10 s respectively. The dimensions of the structural frames are given in Fig. 1. The beams

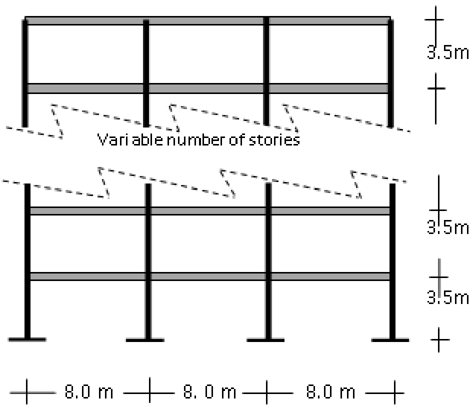

Fig. 1 Schematic structure

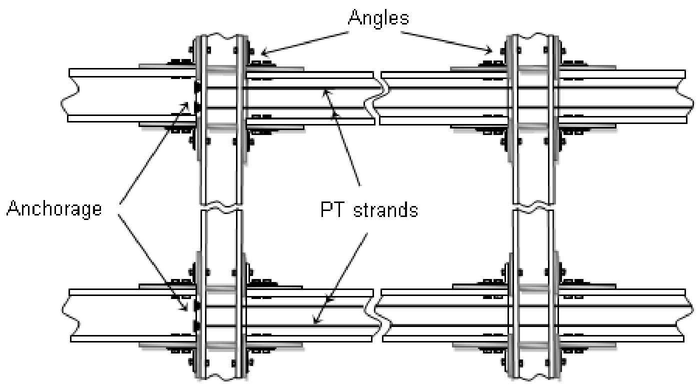

Fig. 2 Basic arrangement of a post-tensioned frame connected with bolted angles

and columns are W sections of A36 steel. A bilinear model with 3% of post-yield stiffness and 3% of critical damping is considered in the analyses. In the design of the connections, steel grade 50 was used for angles, and steel A490 for the screws, which have a diameter of 25 mm. The length of the angles was taken equal to the width of the flange of the beams (b_f). Different angle sizes were tested. In the end, 152×16 mm angles were used in the connection of F4PT model while 152×13 angles were used in the remaining frames. To prevent collapse and local buckling of the flanges, reinforcing plates with a thickness of 25 mm, width equal to b_f and a length 1000 mm, were welded at the ends of the beams. Post-tensioned strands consist of seven wires with an area of 150 mm^2 which withstand a load of 279 kN; they are parallel to the axis of the beam passing through the interior columns and fixed to the outer face of the columns at the ends of the frames. Fig. 2 shows a typical assembly in which the tensioned elements and the energy-dissipating elements for the case of screwed angles can be identified.

2.2 Hysteretic model for post-tensioned connections

The seismic behavior of post-tensioned connections is usually expressed in terms of M-θ_r (moment-relative rotations) curves. Experimental tests with assemblies of beams and columns connected by post-tensioned screwed angles show that the M-θ_r curves present a nonlinear behavior resembling a flag (Ricles *et al*. 2002, Garlock *et al*. 2005, Pirmoz and Danesh 2009, Kim *et al*. 2010), which characterizes the non-linearity, the self-centering capability and the capacity of energy dissipation. Experimental tests with isolated angles, subjected to cyclic and monotonic loads conducted by Shen and Astaneh-Asl (1999) showed a stable cyclic response and good capability of hysteretic energy dissipation. Ultimate strength exceeded 3 times the yield strength and ductility reached values between 8 and 10. The above observations were confirmed in a series of experiments with angles developed by the authors. 152×13 and 152×10 angles with gages (g_a) of 80, 90, 100 and 108 mm were tested for monotonic and cyclic loading for ductility demands of 3, 6, 12 and 18. Results indicate that the number of cycles to failure depends on the ductility demand. In addition, a specific ductility demand value for which the hysteretic energy dissipation capacity of the angles is maximal was observed. For the cases under consideration this ductility demand is 6. Fig. 3(a) shows the results for the particular case of 152×10 angles with g_a = 100 mm. It can be seen that the monotonic curve is the envelope of the curves of the hysteretic cycles.

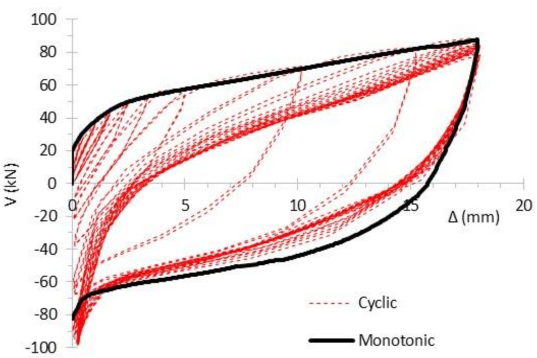

(a) Monotonic and cyclic response

(b) Devices experiments

Fig. 3 Experimental tests

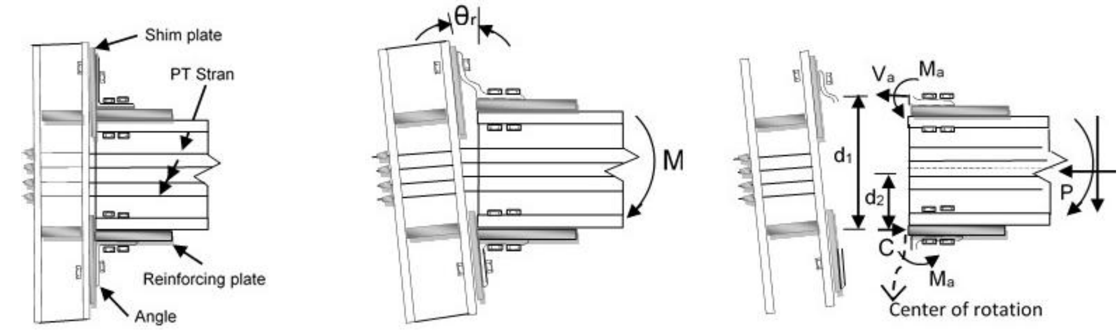

(a) Original configuration (b) Deformed configuration (c) Important parameters

Fig. 4 Connection PT

Moreover, for a given value of ductility demand, the hysteresis loops present a stable behavior. An example of the device used for the experimental tests is shown in Fig. 3(b).

The Figs. 4(a)-(c) show the main elements that are part of a post-tensioned connection, their deformation, and some key parameter of the connection respectively. The lengths d_1 and d_2 in Fig. 4(c) are calculated from the line of the action of the force until the center of the reinforced plate of the compression flange; this point is called the center of rotation (Garlock *et al*. 2005). The strength and stiffness for bending of the post-tensioned connection come from the contribution of the angles of the TS connection and those provided by the post-tensioned cables.

The wires and angles are assumed to work as springs in parallel, the contribution of each one is illustrated separately in Figs. 5(a)-(b); Fig. 5(c) shows the contribution of both. The behavior of the connecting angles is non-linearly since the beginning of the deformation, it is represented by the Richard's model (Richard and Abbott 1975) which mathematically is expressed as

$$M = \frac{(k-k_p)\theta_r}{\left(1+\left|\dfrac{(k-k_p)\theta_r}{M_o}\right|^N\right)^{\frac{1}{N}}} + k_p\theta_r \tag{1}$$

In Eq. (1), k and k_p are the initial and post-yielding stiffness, respectively. N define the curvature zone of transition between elastic and inelastic behavior, and this is estimated with Eq. (2). M_0 is the point where the line with slope k_p intercept the M axis, as shown in Fig. 5(a), and it is computed with Eq. (4). Additional details about these equations can be found in El-Salti (1992).

$$A^N - \left(\frac{B}{f}\right)^N + \left(\frac{1}{f}\right)^N - 1 = 0 \tag{2}$$

In Eq. (2), f takes values from 1.2 to 4, and A and B are estimated with Eq. (3)

$$A = \left[\frac{k-k_p}{\dfrac{M_a}{\theta_a} - k_p}\right] \qquad B = \left[\frac{k-k_p}{\dfrac{M_b}{\theta_b} - k_p}\right] \tag{3}$$

were, the points (M_a, θ_a) *y* (M_b, θ_b) are located before and after the knee of the curve respectively, with $\theta_b > f\theta_a$.

The expression to calculate M_0 is

$$M_0 = \frac{(k - k_p)\theta_a}{(A^N - 1)^{\frac{1}{N}}} \tag{4}$$

The above equations were automatized in the PRCNN computer program (Richard, 1993). With the dimensions and the material of the TS connection, the parameters k, k_p, M_0 *y* N (called Richard parameter) of the Eq. (1) can be obtained by using this program.

The tendons are designed to remain elastic under the earthquakes. Thus, the behavior of the tendons is linear and it is calculated with Eq. (5), where M_s is resistant moment of the connection produced by the tendons. M_d named decompression moment is calculated with Eq. (6), and it is the bending moment associated to the opening of the connection, which is a function of the resulting initial tension in the tendons (T_0), d_2 (see Fig. 4(c)) is the distance from the center of rotation to the action line of T_0. The contribution of the tendons to the stiffness of the connection is estimated with Eq. (7), where k_s is the axial stiffness of the group of tendons, and d_2 was already defined. A plot of the Eq. (5) is shown in Fig. 5(b).

$$M_s = M_d + k_{s\theta}\theta_r \tag{5}$$

$$M_d = T_0 d_2 \tag{6}$$

$$k_{s\theta} = 2k_s d_2^2 \tag{7}$$

The hysteretic model of the complete connection is obtained from the superposition of Eq. (1) and (5), which results in Eq. (8). Eq. (8) corresponds to the monotonic behavior of the connection

$$M = M_d + \frac{(k - k_p)\theta_r}{\left[1 + \left|\frac{(k - k_p)\theta_r}{M_o}\right|^N\right]^{\frac{1}{N}}} + (k_p + k_{\theta S})\theta_r \tag{8}$$

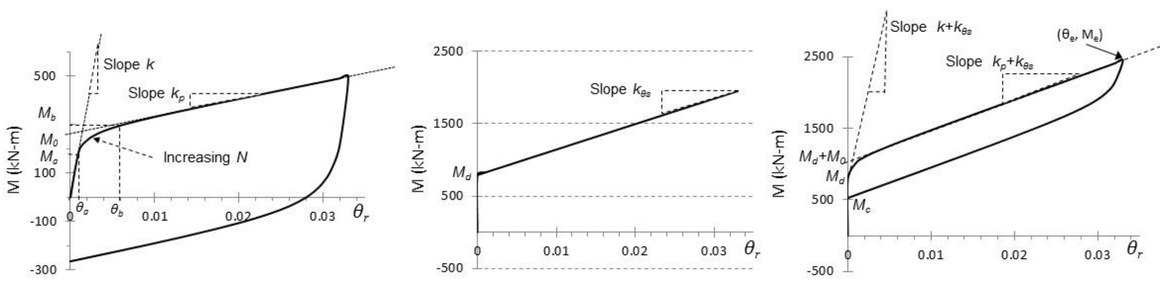

(a) Angles (b) Tendons (c) Angles + tendons

Fig. 5 Contribution of angles and tendons

For unloading the following equation is used

$$M = M_e - \frac{(k-k_p)(\theta_e-\theta_r)}{\left[1+\left|\frac{(k-k_p)(\theta_e-\theta_r)}{\varphi M_o}\right|^N\right]^{\frac{1}{N}}} - (k_p+k_{\theta S})(\theta_e-\theta_r) \tag{9}$$

The parameter φ in Eq. (9) defines the magnitude of the closing moment of the connection (M_c), which must be greater than zero in order to insure complete closure of the connection after getting complete unloading; moreover, this parameter largely defines the E_H dissipation capacity of the connection (enclosed area). In the selected cases here studied a value equals with 4 was appropriated for φ to fit with good accuracy the experimental results. M_e and θ_e are the maximum values reached in each load cycle.

To validate Eqs. (8) and (9) the experimental results of two connections are compared. The first designed as L152-10-g100, is a connection constituted by L152×10 angles, with 152 mm of length and gauge of 100 mm, and a W18×55 beam with reinforced plates in the flanges of 25 mm of thick and steel A36. Four tendons of 100 mm^2 of area and maximum capacity of 186 kN were used, with length of 8.46 m. In order to be used in the analytical model of the connections, the forces and displacements obtained from the test illustrated in Fig. 3(a) are converted to moments and relative rotations with the equations $M = V\,d_1$, and $\theta_r = \Delta/d_1$. In this case d_1 = 520.3 mm and d_2 = 243 mm. The curves M-θ_r obtained are shown in Fig. 6(a) with dotted line, while the continuous lines are the curves obtained with Eqs. (8) and (9). Equivalent plots are shown in Fig. 6(b) together with experimental results of the 36s-20-P specimen published by Garlock *et al*. (2005). In both cases k,

Table 1 Properties of the connections

Connection	k (kN-m/Rad)	k_p (kN-m/Rad)	M_0 (kN-m)	N	$k_{\theta s}$ (kN-m/Rad)	M_d (kN-m)	φ
L152-10-g100	11694	1164	11.42	2	1117	72.2	4
36S-20-p	274000	19200	354	2	24600	1490	4

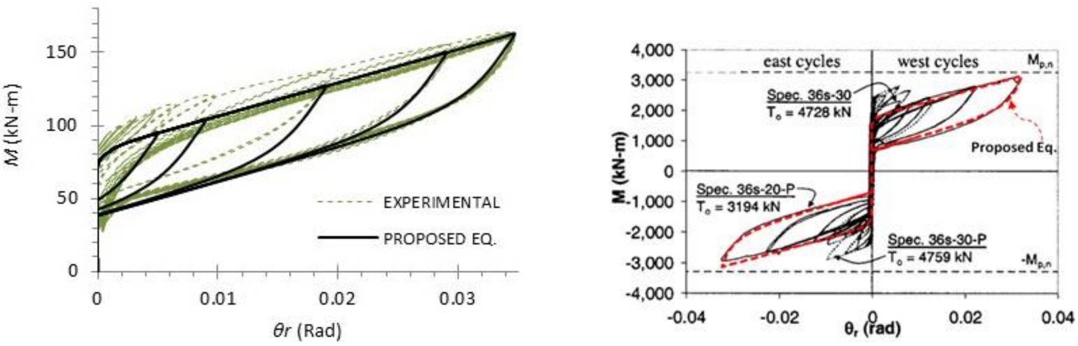

(a) Proposed equations and experimental results (b) Proposed equations and Garlock results

Fig. 6 Comparison of the *M*-*θr* curves of Eqs. (8) and (9) with the experimental results

k_p, N *y* M_0 were obtained with PRCONN (Richard 1993), M_d and K_{0s} are estimated with Eqs. (6) and (7), respectively, all the above parameters are shown in Table 1.

3. Seismic ground motions

The building models described in Section 2.1 were subjected to 30 narrow-band long duration ground motions. The narrow-band earthquakes particularly affect structures within a short interval of periods (especially those suffering of softening or with structural periods close to the period of

Table 2 Ground motion records

Record	Date	Magnitude	Station	A_{ms} (cm/s²)	V_{ms} (cm/s)	Duration (s)
1	19/09/1985	8.1	SCT	178	59.5	164
2	21/09/1985	7.6	Tlahuac deportivo	48.7	14.6	109
3	25/04/1989	6.9	Alameda	45	15.6	93
4	25/04/1989	6.9	Garibaldi	68	21.5	106
5	25/04/1989	6.9	SCT	44.9	12.8	108
6	25/04/1989	6.9	Sector Popular	45.1	15.3	118
7	25/04/1989	6.9	Tlatelolco TL08	52.9	17.3	92
8	25/04/1989	6.9	Tlatelolco TL55	49.5	17.3	84
9	14/09/1995	7.3	Alameda	39.3	12.2	108
10	14/09/1995	7.3	Garibaldi	39.1	10.6	150
11	14/09/1995	7.3	Liconsa	30.1	9.62	130
12	14/09/1995	7.3	Plutarco Elías Calles	33.5	9.37	97
13	14/09/1995	7.3	Sector Popular	34.3	12.5	157
14	14/09/1995	7.3	Tlatelolco TL08	27.5	7.8	125
15	14/09/1995	7.3	Tlatelolco TL55	27.2	7.4	99
16	09/10/1995	7.5	Cibeles	14.4	4.6	105
17	09/10/1995	7.5	CU Juárez	15.8	5.1	125
18	09/10/1995	7.5	Centro urbano Presidente Juárez	15.7	4.8	106
19	09/10/1995	7.5	Córdoba	24.9	8.6	124
20	09/10/1995	7.5	Liverpool	17.6	6.3	126
21	09/10/1995	7.5	Plutarco Elías Calles	19.2	7.9	171
22	09/10/1995	7.5	Sector Popular	13.7	5.3	141
23	09/10/1995	7.5	Valle Gómez	17.9	7.18	79
24	11/01/1997	6.9	CU Juárez	16.2	5.9	77
25	11/01/1997	6.9	Centro urbano Presidente Juárez	16.3	5.5	122
26	11/01/1997	6.9	García Campillo	18.7	6.9	102
27	11/01/1997	6.9	Plutarco Elías Calles	22.2	8.6	115
28	11/01/1997	6.9	Est. # 10 Roma A	21	7.76	111
29	11/01/1997	6.9	Est. # 11 Roma B	20.4	7.1	123
30	11/01/1997	6.9	Tlatelolco TL08	16	7.2	76

the soil). In fact, these records demand large amounts of energy to structures compared to broad-band records (Terán and Jirsa 2007). The ground motions were recorded in sites where the period of the soil was close to two seconds and the more severe damage on structures was observed, during the 1985 Mexico City Earthquake. Table 2 shows the magnitude, acceleration, velocity and duration of each of the seismic records considered. The duration was computed according with Trifunac and Brady (1975).

4. Hysteretic energy distribution in the frames

One of the requirements in the design of steel MRFs with PT connections is to concentrate plastic deformations in the angles of the connections while beams and columns remain essentially elastic under strong earthquakes, in such a way that the angles can be easily replaced in the case of excessive structural damage. To determine the E_H, incremental dynamic analysis is performed for each frame subjected to the a set of 30 seismic records scaled at different values of seismic intensity in terms of spectral acceleration at fundamental period of vibration of the structure $Sa(T_1)$. The seismic intensity varies from 0.1 g to 1.0 g with increments of 0.1 g. The RUAUMOKO program (Carr 2011) was used for non-linear, step-by-step dynamic analysis. To show how the demands of γ and E_H are distributed, the F10PT model is subjected to Record 1 scaled to $Sa(T_1)$ = 0.9 g. The maximum inter-story drift demands are shown in Fig. 7, the maximum value is 0.021 and occurs at 4th floor. Fig. 8(a) shows the E_H dissipated by the structural elements; the connections dissipate 65.6% and the columns 34.4%. The beams do not dissipate energy, implying

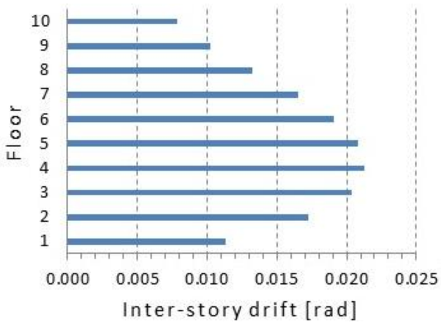

Fig. 7 Inter-story drift in F10PT under record 1 scaled to $Sa(T_1)$ = 0.9 g

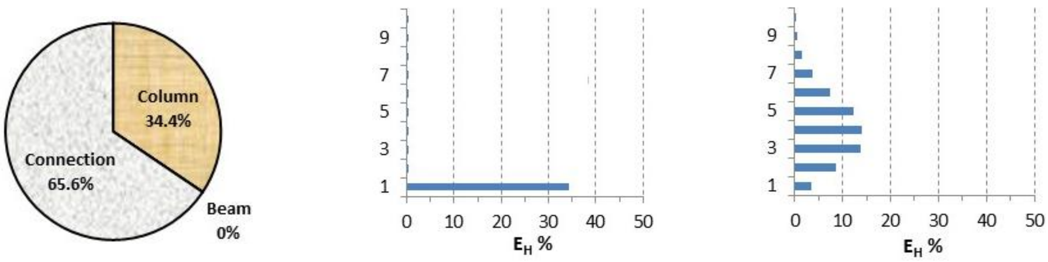

(a) E_H total (b) Distribution in columns (c) Distribution in connections

Fig. 8 E_H in F10PT under record 1 scaled to $Sa(T_1)$ = 0.9 g that there is no plastic deformation on them. Fig. 8(b) shows the E_H dissipated by the columns for each inter-story; it is observed that the base columns are the only ones that dissipate energy, the reason for this is that the supports of these columns are fixed, resulting in the formation of plastic hinges on that location even for moderate seismic demands. The connections dissipate energy on every floor, being larger on Floors 3, 4 and 5, as shown in Fig. 8(c). A similar distribution is observed for γ (Fig. 7) and E_H (Fig. 8(c)).

The E_H is now estimated for a target value of γ. Each PT frame model, is subjected to all earthquakes, scaled to different levels of seismic intensity, then the values of γ and the corresponding value of $Sa(T_1)$ are plotted and the median of maximum inter-story drift ($\bar{\gamma}$) is calculated. From this curve, the required value of $Sa(T_1)$ to produce a given target value of median maximum inter-story drift can be calculated; that is, the relationship between seismic intensity and the median value of the maximum inter-story drift is obtained. Fig. 9 shows the results for the F10PT model, discrete values of γ are obtained for the thirty earthquakes scaled to $Sa(T_1)$ varying from 0.1 to 1.0 g. The solid line represents $\bar{\gamma}$, from which it is possible to read the values of $Sa(T_1)$ for specific values of $\bar{\gamma}$. Table 3 shows the magnitudes of $Sa(T_1)$ for values of $\bar{\gamma}$ for all models; it can be seen that for a given $\bar{\gamma}$, the seismic intensity magnitude increases as the height of the building increases.

Table 4 contains the E_H dissipated by the columns, beams and connections corresponding to different demands of maximum drift. The results are presented for the average values of E_H, in percentage, demanded by the 30 earthquakes scaled to the same seismic intensity normalized with respect to the total E_H. The participation of the beams is very small, implying that the connections and the columns mostly dissipate the energy. It is observed that the participation of connections

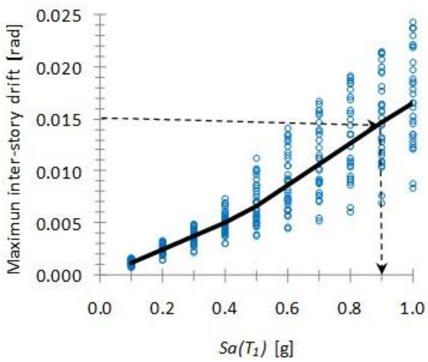

Fig. 9 Median maximum inter-story drift obtained for model F10PT

Table 3 Relation between maximum inter-story drift and the seismic intensity

$\bar{\gamma}$	$Sa(T_1)$				
	F4PT	F6PT	F8PT	F10PT	F14PT
0.005	0.3 g	0.4 g	0.4 g	0.4 g	0.7 g
0.010	0.5 g	0.7 g	0.6 g	0.7 g	*
0.015	0.7 g	0.9 g	0.8 g	0.9 g	*
0.020	0.8 g	1.0 g	1.0 g	*	*

*Not obtained because the $Sa(T_1)$ was limited to 1.0 g

Table 4 Total E_H dissipated by columns, beams and connections corresponding to various demands of maximum inter-story drift

Frame	Drift	E_H %		
		Columns	Beams	Connections
F4PT	γ = 0.005	0.0	0.0	0.0
	γ = 0.010	69.8	0.5	29.8
	γ = 0.015	70.9	0.4	28.7
	γ = 0.020	69.0	3.2	27.8
F6PT	γ = 0.005	0.0	0.0	0.0
	γ = 0.010	45.9	0.4	53.6
	γ = 0.015	51.6	0.6	47.8
	γ = 0.020	52.5	1.3	46.3
F8PT	γ = 0.005	0.0	0.0	100.0
	γ = 0.010	22.6	0.0	77.4
	γ = 0.015	36.7	0.3	63.0
	γ = 0.020	42.9	0.7	56.4
F10PT	γ = 0.005	0.0	0.0	100.0
	γ = 0.010	2.4	1.1	96.5
	γ = 0.015	19.0	0.4	80.6
F14PT	γ = 0.005	0.0	0.0	100.0

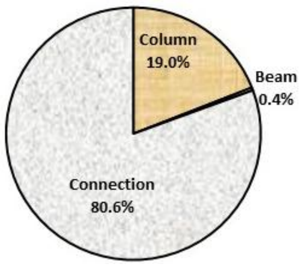

Fig. 10 E_H dissipated by connections, beams and columns in F10PT for a target median γ = 0.015

increases and the participation of the columns decreases as the number of levels increases.

Fig. 10 shows the average dissipated E_H in the F10PT model for a maximum inter-story drift demand of 0.015 (earthquakes escalated to $Sa(T_1)$ = 0.9 g). It is observed that 80.6% of the total E_H is dissipated by the connections, 19% by columns and only 0.4% by beams. Fig. 11 shows how the demands of E_H are distributed in columns, beams and connections for each level. The total energy dissipated by the columns is concentrated in the first story, because the columns are fixed at the base, as previously explained. The distribution of E_H in the beams is negligible. The connections dissipate energy on every floor, being larger on Floors 3 and 5 and smaller on Floors 8, 9 and 10. In this case, a lognormal distribution of E_H through the height is appropriate. Similar results were observed for the other models, where it was also observed that the participation of the connections in dissipating hysteretic energy increases when the number of stories increases; this is expected

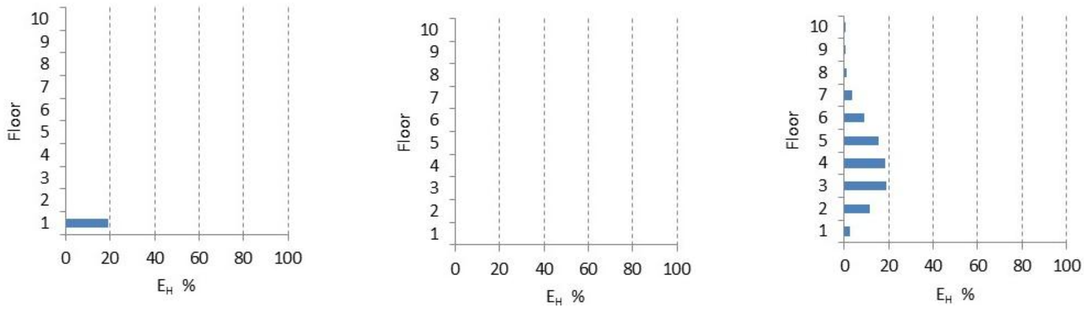

(a) Columns (b) Beams (c) Connections

Fig. 11 E_H dissipated in each level of F10PT by columns, beams and connections for a target median γ = 0.015

since the number of connections increases while the number of columns that dissipate energy remain the same (at the base).

5. Hysteretic energy distribution factors (F_{EH})

The distribution of hysteretic energy demands in the structures is an important aspect that needs to be considered in seismic design methodologies based on this parameter. Since γ is the parameter commonly used to achieve satisfactory seismic performance, it is desirable to have an expression for estimating hysteretic energy demands and their distribution along the height as a function of γ. In order to obtain the distribution of hysteretic energy through height, the structures were subjected to all the seismic records under consideration which are scaled until a specific value of the median maximum inter-story drift is obtained. The procedure for estimating the F_{EH} is as follows:

Step 1. Incremental dynamic analysis of the steel frame is carried out using all the seismic records scaled to different levels of seismic intensity in terms of $Sa(T_1)$.

Step 2. The median maximum inter-story drift ($\bar{\gamma}$) is plotted and the required value of $Sa(T_1)$ that produces the target value of maximum inter-story drift is obtained.

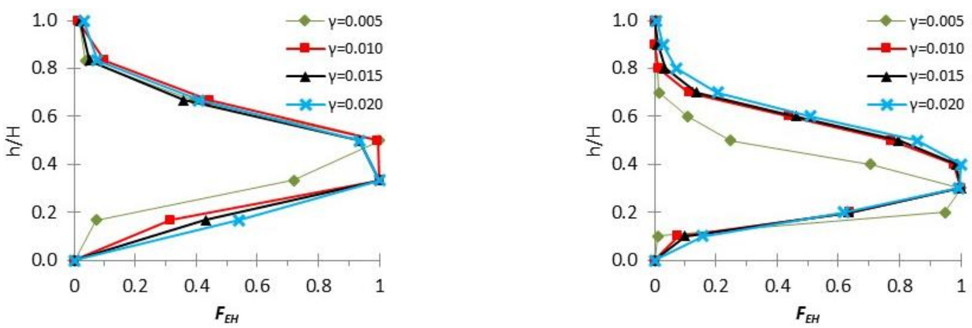

(a) F6PT (b) F10PT

Fig. 12 Distribution of F_{EH} along the height for different values of γ

Step 3. The hysteretic energy distribution is obtained for values of specific seismic intensity for each seismic record; then the average hysteretic energy on each floor is calculated. Hysteretic energy distribution factors F_{EH} are obtained as the ratio of the average hysteretic energy of each floor to the average hysteretic energy of the floor undergoing the largest energy demand.

Fig. 12 shows the F_{EH} values for each floor at several levels of inter-story drift demands of the F6PT and F10PT models; h/H is the height of each floor normalized by the total height of the structure (H) relative to the ground level. It is observed that the distribution of E_H through height is essentially log-normal for different levels of inter-story drift demand, the same occurs for the F4PT, F8PT and F14PT models. It can also be observed that an increment in the inter-story drift causes a greater participation of the upper floors in plastic energy dissipation.

6. Equation for the estimation of F_{EH}

As stated early the distribution of dissipated hysteretic energy along the height of post-tensioned regular steel frames can reasonably be represented by a log-normal distribution. By using the result of all the models Eq. (10) is proposed to estimate F_{EH} as a function of building height and the maximum inter-story drift demand.

$$F_{EH} = \frac{1}{f_1(\gamma)\left(\frac{h}{H}\right)} \exp\left\{-\frac{1}{2}\left[\frac{\ln\left(\frac{h}{H}\right) - \ln(f_2(\gamma))}{f_3(\gamma)}\right]^2\right\} \tag{10}$$

In Eq. 10, the parameters $f_1(\gamma)$, $f_2(\gamma)$ and $f_3(\gamma)$, which are estimated with Eqs. (11), (12) and (13), respectively, are a function of the maximum inter-story drift demand, and are obtained from regression analysis by using the F_{EH} values of all frames.

$$f_1(\gamma) = 17.002\gamma + 2.411 \tag{11}$$

$$f_2(\gamma) = 2.944\gamma + 0.353 \tag{12}$$

$$f_3(\gamma) = 14.786\gamma + 0.269 \tag{13}$$

Eq. (10) is plotted with solid lines in Figs. 13(a)-(d), together with the discrete values of F_{EH} obtained for maximum drifts of 0.005, 0.010, 0.015 and 0.020 for all frames. It is observed that the number of levels or structural period of vibration of the frames does not affect the shape of the distribution of E_H through height. It is also noted also that the largest energy demands are obtained for $0.25 \leq h/H \leq 0.5$. Figs. 13(a)-(d) suggests that the values of F_{EH} can be calculated with the proposed equation with good accuracy. Table 5 shows the F_{EH} values calculated with Eq. (10) for different demands of inter-story drift; it can be seen that the peak demand of E_H is given for h/H = 0.3 for all values of γ. It is also observed that the F_{EH} values increase as the values of γ increase. Eq. (10), together with the values given by Eqs. (11), (12) and (13), is fitted with good accuracy to the

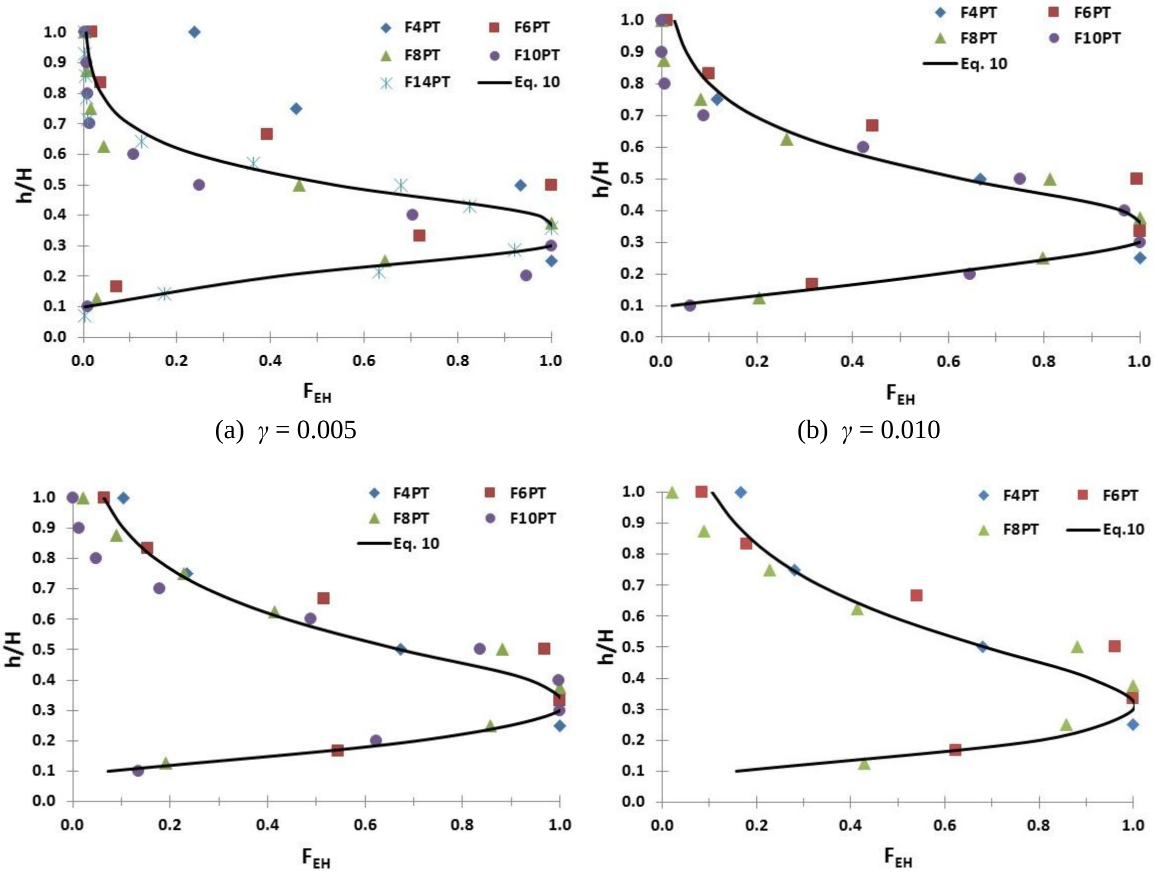

(a) $\gamma = 0.005$ (b) $\gamma = 0.010$

(c) $\gamma = 0.015$ (d) $\gamma = 0.020$

Fig. 13 Comparison of F_{EH} using Eq. (10) with the result of the numerical analysis for all the models and several values of γ

Table 5 F_{EH} calculated using Eq. (10)

h/H	$\gamma = 0.005$	$\gamma = 0.010$	$\gamma = 0.015$	$\gamma = 0.020$
0.1	0.003	0.022	0.072	0.157
0.2	0.414	0.578	0.706	0.802
0.3	1.000	1.000	1.000	1.000
0.4	0.972	0.963	0.938	0.908
0.5	0.536	0.630	0.672	0.685
0.6	0.241	0.360	0.439	0.485
0.7	0.098	0.193	0.275	0.334
0.8	0.038	0.101	0.169	0.228
0.9	0.015	0.052	0.104	0.155
1	0.006	0.027	0.064	0.106

distribution of E_H obtained from the step-by-step nonlinear dynamic analysis, indicating that the expression can reasonably be used to estimate the energy distribution through the height of regular PT steel moment resisting frames.

7. Conclusions

The capacity of self-centering, the concentration of damage on elements which can be easily replaceable, and the ability to dissipate energy, of post-tensioned moment resisting steel frames make them a viable alternative for steel buildings in seismic prone-areas. The maximum inter-story drift (γ) is one of the main parameters used in seismic design codes to ensure a satisfactory seismic performance of structures. However, this parameter does not explicitly contemplate the effect of accumulated structural damage caused by plastic deformation. In this paper, the seismic behavior of post-tensioned moment resisting steel frames is studied in terms of dissipated hysteretic energy, due to the ability of this parameter to represent cumulative damage. Five steel frames under the action of 30 ground motion recorded on soft soil sites are used in the study.

An expression is proposed to estimate energy dissipated by hysteretic behavior of post-tensioned semi-rigid connections. The equation, which models the hysteretic cycles of this type of connections, exhibits an excellent accuracy when compared with experimental results.

The distribution and demands of hysteretic energy (E_H) in beams, columns and connections were determined for different demands of γ. It is observed that E_H varies with γ, and that, except for the columns at the base, E_H is dissipated by plastic deformation of the angles in the connection. The other structural components remain elastic even for large demands of the inter-story drift. It is observed in all cases a log-normal distribution of E_H with height. The greatest demand of E_H occurs between 0.25 and 0.5 of height. The tallest buildings exhibit a smoother variation of E_H through height for all inter-story drift levels. This distribution does not depend on the fundamental periods of the models. In the case of the upper floors, the hysteretic energy demands tend to increase as the maximum inter-story drift increases. By using these results an equation is proposed to calculate the hysteretic energy distribution factors (F_{EH}) in terms of the relative height of the stories (h/H) and γ. It is shown that the proposed equation can be used to accurately estimate the distribution of E_H demands in post-tensioned moment resisting steel frames.

Acknowledgments

This study was supported by Secretaría de Educación Publica (DSA/103.5/15/7085), Universidad Nacional Autónoma de México (DGAPA-UNAM under project IN-102114), and by Universidad Autónoma de Sinaloa (under grant PROFAPI 2014/109). Any opinions, findings, conclusions, or recommendations expressed in this publication are those of the authors and do not necessarily reflect the views of the sponsors.

References

Akbas, B., Shen, J. and Hao, H. (2001), "Energy approach in performance-based design of steel moment resisting frames for basic safety objective", *Struct. Des. Tall Build.*, **10**(3), 193-217.

Akiyama, H. (1985), *Earthquake-Resistant Limit-State Design for Buildings*, University of Tokyo Press, Tokyo, Japan.

Arias, A. (1970), “A measure of earthquake intensity”, Seismic Design for Nuclear Power Plants; (R.J. Hansen Eds.), MIT Press, Cambridge, MA, USA, pp. 438-483.

Bojórquez, E. and Rivera, J.L. (2008), “Effects of degrading models for ductility and dissipated hysteretic energy in uniform annual failure rate spectra”, *Proceedings of the 14th World Conference on Earthquake Engineering*, Beijing, China, October.

Bojórquez, E. and Ruiz, S.E. (2004), “Strength reduction factors for the valley of Mexico taking into account low cycle fatigue effects”, *Proceedings of the 13th World Conference on Earthquake Engineering*, Vancouver, Canada, Paper 516. (CD-ROM)

Bojórquez, E., Ruiz, S.E. and Terán-Gilmore, A. (2008), “Reliability-based evaluation of steel structures using energy concepts”, *Eng. Struct.*. **30**(6), 1745-1759.

Bojórquez, E., Reyes-Salazar, A., Terán-Gilmore, A. and Ruiz, S.E. (2010), “Energy-based damage index for steel structures”, *Steel Compos. Struct., Int. J.*, **10**(4), 343-360.

Carr, A. (2011), “RUAUMOKO”, *Inelastic Dynamic Analysis Program*; University of Cantenbury, Department of Civil Engineering, Christchurch, New Zealand.

Choi, H. and Kim, J. (2006), “Energy-based seismic design of buckling-restrained braced frames using hysteretic energy spectrum”, *Eng. Struct.*, **28**(2), 304-311.

Choi, H. and Kim, J. (2009), “Evaluation of seismic energy demand and its application on design of buckling-restrained braced frames”, *Struct. Eng. Mech., Int. J.*, **31**(1), 93-112.

Choi, B.J. and Shen, J.H. (2001), “The establishing of performance level thresholds for steel moment-resisting frame using an energy approach”, *Struct. Des. Tall Build.*, **10**(1), 53-67.

Christopoulos, C. and Filiatrault, A. (2002), “Seismic response of posttensioned energy dissipating moment resisting steel frames”, *Proceedings of the 12th European Conference on Earthquake Engineering*, London, UK, September.

Christopoulos, C., Filiatrault, A. and Uang, C.M. (2002), “Self-centering post-tensioned energy dissipating (PTED) steel frames for seismic regions”, Report No. SSRP-2002/06; Division of Structural Engineering, University of California, San Diego, CA, USA.

Christopoulos, C., Filiatrault, A. and Uang, C.M. (2003), “Seismic demands on post-tensioned energy dissipating moment-resisting steel frames”, *Proceedings of 4th International Conference on the Behavior of Steel Structures in Seismic Areas* (*STESSA*), Naples, Italy, June.

Chung, C.C., Tsai, K.C. and Yang, W.C. (2009), “Self-centering steel connection with steel bars and a discontinuous composite slab”, *Earthquake Engng Struc. Dyn.*, **38**(4), 403-422.

Cosenza, E. and Manfredi, G. (1996), “Seismic design based on low cycle fatigue criteria”, *Proceedings of XI World Conference on Earthquake Engineering*, Paper 1141, Acapulco, México, June. (CD)

El-Salti, M.Kh. (1992), “Design of frames with partially restrained connections”, Ph.D. Dissertation; The University of Arizona, Tucson, AZ, USA.

Garlock, M., Ricles, J. and Sause, R. (2005), “Experimental studies on full-scale post tensioned steel connections”, *J. Struct. Eng., ASCE,* **131**(3), 438-448.

Garlock, M., Sause, R. and Ricles, J. (2007), “Behavior and design of posttensioned stell frames system”, *J. Struct. Eng., ASCE*, **133**(3), 389-399.

Garlock, M., Sause, R. and Ricles, J. (2008), “Influence of design parameter on seismic response of post-tensioned steel MRF systems”, *Eng. Struct.*, **30**(4), 1037-1047.

Hancock, J. and Bommer, J.J. (2006), “A state-of-knowledge review of the influence of strong-motion durationon structural damage”, *Earthq. Spectra*, **22**(3), 827-845.

Hu, X. and Zhang, Y. (2013), “Ductility demand of partially self-centering structures under seismic loading: SDOF systems”, *Earthq. Struct.*, **4**(4), 365-381.

Kim, H.J. and Christopoulos, C. (2009), “Seismic design procedure and seismic response of post-tensioned self-centering steel frames”, *Earthq. Eng. Struct. Dyn.*, **38**(3), 355-376.

Kim, H.J., Ghaboussi, J. and Elnashai, A.S., (2010), “Mechanical and informational modeling of steel beam-to-column connections”, *Eng. Struct.*, **32**(2), 449-458.

López-Barraza, A., Bojórquez, E., Ruiz, S.E. and Reyes-Salazar, A. (2013), “Reduction of maximum and residual drifts on post-tensioned steel frames with semi-rigid connections”, *Adv. Mater. Sci. Eng.*, **2013**, ID 192484. DOI:10.1155/2013/192484

Pirmoz, A. and Danesh, F. (2009), "The seat angle role on moment-rotation response of bolted angle connection", *Electron. Struct. Eng.*, **9**, 73-79.

MCBC (2004), Reglamento de Construcciones del Distrito Federal. [In Spanish]

Richard, R.M. (1993), PRCONN manual; RMR Design Group, Tucson, AZ, USA.

Richard, R.M. and Abbott, B.J. (1975), "Versatile elastic-plastic stress-strain formula", *J. Eng. Mech. Div.*, **101**(4), 511-515.

Ricles, J.M., Sause, R., Garlock, M.M. and Zhao, C. (2001), "Posttensioned seismic-resistant connections for steel frames", *ASCE J. Struct. Eng.*, **127**(2), 113-121.

Ricles, J.M., Sause, R., Peng, S.W. and Lu, L.W. (2002), "Experimental evaluation of earthquake resistant posttensioned steel connections", *ASCE J. Struct. Eng.*, **128**(7), 850-859.

Ricles, J.M., Sause, R., Lin, Y.C. and Seo, C.Y. (2010), "Self-centering moment connections for damage-free seismic response of steel MRFs", *2010 Structures Congress ASCE*, Orlando, FL, USA, May, pp. 955-966.

Shen, J., and Astaneh-Asl, A. (1999), "Hysteretic behavior of bolted angle connections", *J. Construct. Steel Res.*, **51**(3), 201-218.

Terán-Gilmore, A. (1996), "Performance-based earthquake-resistant design of framed buildings using energy concepts", Ph. D. Dissertation; University of California, Berkeley, CA, USA.

Terán-Gilmore, A. (2001), "Consideraciones del uso de la energía plástica en el diseño sísmico", *Revista de ingeniería Sísmica*, *SMIS*, **65**, 81-110.

Terán-Gilmore, A. and Jirsa, J.O. (2005), "A damage model for practical seismic design that accounts for low cycle fatigue", *Earthq. Spectra*, **21**(3), 803-832.

Terán-Gilmore, A. and Jirsa, J.O. (2007), "Energy demands for seismic design against low-cycle fatigue", *Earthq. Eng. Struct. Dyn.*, **36**(3), 383-404.

Tong, G., Lianglong, S. and Guodong, Z. (2011), "Numerical simulation of the seismic behavior of self-centering steel beam-column connections with bottom flange friction devices", *Earthq. Eng. Eng. Vib.*, **10**(2), 229-238.

Trifunac, M.D. and Brady, A.G. (1975), "A study of the duration of strong earthquake ground motion", *Bull. Seismol. Soc. Am.*, **65**(3), 581-626.

Uang, C.M. and Bertero, V.V. (1990), "Evaluation of seismic energy in structures", *Earthq. Eng. Struct. Dyn.*, **19**(1), 77-89.

Wolski, M., Ricles, J.M. and Sause, R. (2009), "Experimental study of self-centering beam-column connection with bottom flange friction device", *ASCE J. Struct. Eng.*, **135**(5), 479-488.

Zhou, Z., He, X.T., Wu, J., Wang, C.L. and Meng, S.P. (2014), "Development of a novel self-centering buckling-restrained brace with BFRP composite tendons", *Steel Compos. Struct., Int. J.*, **16**(5), 491-506. DOI: 10.12989/scs.2014.16.5.491

CC